

Joint Deployment of Macro- and Microcells in UTRAN FDD Networks

Patrick Herhold, Wolfgang Rave, Gerhard Fettweis

Dresden University of Technology · Mannesmann Mobilfunk Chair for Mobile Communications
Helmholtzstrasse 18 · D-01062 Dresden · Germany

Email: {herhold,rave,fettweis}@ifn.et.tu-dresden.de · Phone/Fax: +49 (351) 463-34660/-37255

ABSTRACT— *In recent years, the WCDMA radio network performance has been studied with the focus on deployment of sectorized macrocells. The macrocellular layer will be enhanced by microcell base stations within the next two years. As the class of micro-FDD Node Bs differs in some important aspects from typical macro Node Bs, it is of interest to investigate the impact of these differences and to study effective means of network optimization. To this end, we first analyze the mutual interferences between macro- and microcells and show how they affect the joint capacity of both cell types. Next, system-level simulations are performed to demonstrate the influence of various parameters such as the admissible uplink load and common channel power as well as antenna patterns and their downtilt. Finally, a case study comprising realistic site positions and propagation data is performed for verification of the general results.*

1 INTRODUCTION

A GAINST the background of the immense financial efforts necessary for deploying UMTS FDD networks, it is crucial to utilize the available spectrum most efficiently. Second generation systems have shown that microcells are capable of successfully enhancing network capacity as part of *hierarchical cell structures (HCS)*.

Likewise, microcells in UMTS FDD networks are to be deployed in urban areas characterized by high traffic densities. Operators in these areas will fully utilize their available spectrum for the macrocellular layer, so that the need for operating all cells of the HCS system on the *same* carriers arises. Most of the micro FDD Node Bs available in 2002 will serve a single sector on one carrier.

Macrocells and microcells of the FDD system, each forming a layer of cells, impose mutual interferences to each other. The optimum situation is achieved if the mutual interferences between these two layers are minimum. This and other aspects have been investigated for IS-95 recently [1, 2]. However, due to the fundamental differences between 2G and 3G CDMA radio systems it becomes necessary to study the scale of the mutual interferences in UTRAN networks. In this work, we concentrate on FDD networks and determine which parameters are suitable for network optimization in

WCDMA HCS systems. Problems related to TDD Node Bs, which will provide additional capacity for picocellular applications, are not discussed in this paper.

The paper is organized as follows. We start with an analysis of the mutual interferences in section 2. Following a brief description of the static simulation tool and the underlying assumptions in section 3, we discuss possible optimization methods and present related simulation results in section 4. The paper concludes in section 5.

2 ANALYSIS

2.1 Mutual Uplink Interferences

The analysis is based on the uplink signal-to-interference-and-noise ratio (SINR) assuming a single-service network with permanently transmitting mobiles. The system is assumed to consist of multiple macrocells and a single microcell. Basically we follow the approach taken in [1].

In general, there exist three types of multiple access interference (MAI) contributions in a cell: the intracell MAI from users in the own cell, the intercell MAI from neighboring cells of the same layer, and the cross-layer MAI imposed by cells of the other layer.

In a macrocell, the UL intracell MAI for the detection of a single user's signal can be expressed as

$$P_M^{intra} = P_M^r (\nu_M C_0 - 1), \quad (1)$$

where P_M^r is the required received signal power per user at the macrocell site and ν_M is the fractional load of this cell with respect to the pole capacity C_0 ($0 \leq \nu_M \leq 1$). Hence, ν_M represents the throughput-based load factor. C_0 is the pole capacity of an isolated cell in terms of number of users, so that the product $\nu_M C_0$ corresponds to the number of users currently being connected to the BS.

Similarly, we define for the microcell P_μ^r as the required received signal power at the microcell site and ν_μ as its fractional load. Note that the required powers P_M^r and P_μ^r are a function of the fractional loads ν_M and ν_μ . The powers are adjusted by outer and inner loop power control according to the target SINR and the current interference situation.

Assuming equal loading conditions in neighboring macrocells, the intercell MAI P_{MM} can be described as a certain multiple of the intracell MAI P_M^{intra} by the macro-to-macro intercell interference ratio F_{MM} . Similarly, the interference caused by users in the embedded microcell, $P_{\mu M}$, is found from the required received powers at the microcell site, multiplied by the numbers of users and weighted by a factor $F_{\mu M}$. This factor $F_{\mu M}$ relates the expected fraction of the MAI caused by transmissions in the microcell to the intracell MAI of the macrocell. The intercell interference powers at the macrocell are then

$$P_{MM} = P_M^r \nu_M C_0 F_{MM}, \quad (2)$$

$$P_{\mu M} = P_\mu^r \nu_\mu C_0 F_{\mu M}. \quad (3)$$

Collecting the interferences (1) to (3), the macrocell UL SINR $\gamma_M = (E_c/N_0)_M$ can now be expressed as

$$\gamma_M = \frac{P_M^r}{P_M^{intra} + P_{MM} + P_{\mu M} + P_N}, \quad (4)$$

where P_N is the receiver noise power.

Likewise, the UL SINR $\gamma_\mu = (E_c/N_0)_\mu$ at a *single* microcell within the macrocellular layer is

$$\begin{aligned} \gamma_\mu &= \frac{P_\mu^r}{P_\mu^{intra} + P_{M\mu} + P_N} \\ &= \frac{P_\mu^r}{P_\mu^r (\nu_\mu C_0 - 1) + \nu_M C_0 P_M^r F_{M\mu} + P_N}. \end{aligned} \quad (5)$$

We now want to express the inherent coupling between (4) and (5) more explicitly. Thus we proceed by deriving expressions for the pole capacity of an isolated cell, in which case $F_{MM} = F_{M\mu} = F_{\mu M} = 0$. For full loading ($\nu \rightarrow 1$), the transmission and interference powers diverge, and thermal noise can be neglected. Assuming equivalent SINRs being requested at both cell types ($\gamma_M = \gamma_\mu = \gamma_{tar}$), the pole capacities of macrocells and microcells are equal and follow

$$C_0 = \frac{1}{\gamma_{tar}} + 1 \simeq \frac{1}{\gamma_{tar}} (\gamma_{tar} \ll 1), \quad (6)$$

where γ_{tar} is the target SINR at chip level.¹ Note that for a non-isolated cell, the load $\nu = 1$ cannot be reached due to the limiting intercell interference from surrounding macrocells.

Using (6) in (5) and solving for ν_μ yields the maximum possible fractional microcell load in the presence of thermal noise and macrocell interference

$$\nu_\mu = 1 - \nu_M F_{M\mu} \frac{P_M^r}{P_\mu^r} - \frac{P_N}{P_\mu^r C_0} + \frac{1}{C_0}. \quad (7)$$

¹The bit-level SINR, E_b/N_0 , is related to γ and the processing gain G by $E_b/N_0 = G \cdot \gamma$.

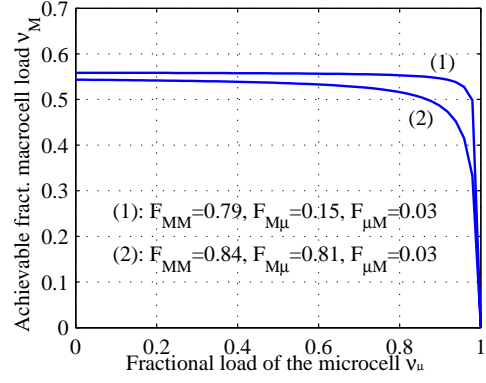


Figure 1: The achievable fractional load of the macrocell as a function of the fractional load in the microcell according to equation (10). The interference ratios have been taken from our simulations. The smaller interference ratios for curve (1) yield a larger achievable fractional load of the macrocell.

For a compact description, we define χ as the ratio of the required received powers at the different cell sites [1], $\chi = P_M^r/P_\mu^r$, and abbreviate the degradation of the achievable loading due to thermal noise power by $\xi_\mu = (P_N/P_\mu^r - 1)/C_0$. Thus, we arrive at an expression for ν_μ in terms of ν_M

$$\nu_\mu = (1 - \xi_\mu) - \nu_M F_{M\mu} \chi. \quad (8)$$

Likewise, using (1) to (3) in (4), we obtain

$$\nu_M = \frac{1}{1 + F_{MM}} \left(1 - \xi_M - \nu_M \frac{F_{\mu M}}{\chi} \right), \quad (9)$$

with $\xi_M = \left(\frac{P_N}{P_M^r} - 1 \right) / C_0$.

By eliminating χ in the preceding equations, the achievable loading ν_M of the macrocell is expressed as a function of the microcell's fractional load ν_μ ,

$$\nu_M = \frac{1 - \xi_M}{1 + F_{MM} + \frac{\nu_\mu}{1 - \xi_\mu - \nu_\mu} F_{\mu M} F_{M\mu}}. \quad (10)$$

The joint capacity $\nu_M + \nu_\mu$ of the HCS system depends on the product of the interference ratios $F_{\mu M}$ and $F_{M\mu}$. A better interference isolation between the layers will cause lower mutual interferences, and total capacity increases. This makes obvious what could have been expected intuitively: the capacity of the HCS system is maximized for $F_{\mu M} F_{M\mu} \rightarrow \min$ and $F_{MM} \rightarrow \min$.

A plot of relation (10) is shown in Fig. 1 for typical values of F that have been obtained from the simulations presented in section 4. These curves depict that the interference coupling of the cells is remarkably weak, i.e. the achievable macrocell load decreases for very high microcell loadings only.

In contrast to IS-95, the ratio χ of the required received powers is automatically adjusted by SINR based power control in 3G networks, thus enabling to benefit from the parallel deployment more easily.

Parameter	Value
Radius of macrocells	500 m
Log-normal shadowing (σ)	8.0 dB
Target SINR E_c/N_0 (γ_{tar})	-14.5 dB
Noise power (P_N)	-106.8 dBm
Receiver noise figure Node B/ UE	3 / 5 dB
Maximum UE transmit power	21 dBm
Total BS Power	(43;33) dBm
Maximum DL DCH power	(30;20) dBm
DL orthogonality factor (α_M)	(0.4;0.06)
Minimum coupling loss (MCL) [5]	(70;53) dB
Antenna height	(40;6) m
Allowed macro UL load ($\eta_{max,M}$)	0.60
Maximum active set size	3
Macro antenna omni: gain	11 dBi
Macro antenna sect.: (gain, HPBW)	(18 dBi, 65°)
Micro omni antenna: gain	2.0 dBi

Table 1: Simulation Parameters. Cell radius, antenna heights and minimum coupling losses are different for the case study. Unless otherwise stated, the value pairs in parenthesis denote the settings for macro- and microcells, respectively.

2.2 Downlink

Due to the similar propagation characteristics for UL and DL and the symmetry of the antenna patterns for the transmit and receive direction, minimum mutual interferences in the UL will correspond to minimum impairments in the DL. A separate analysis for the DL therefore will yield results similar to those obtained for the UL.

3 STATIC SIMULATION SCHEME

3.1 Simulator

A static simulation tool was used to investigate the scale of the mutual interferences and to assess the influence of various parameters on system capacity. Relevant simulation parameters are summarized in Table 1. Soft handover (SHO) has been modeled with perfect combining and link-level gains [3]. These gains result in a reduction of the average transmit power, caused by the improved robustness of multiple active links against fast fading.² Furthermore, a perfect power control (PC) algorithm was implemented [4]³, which here was operated with the constraints imposed by limited transmit powers in both UL and DL.

A simulation consists of numerous snapshots, the results of which are averaged to obtain reliable statistics. Each snapshot represents a single realization of a random distribution of users and log-normal shadowing. In a snapshot, cells are filled with users until either their maximum allowed UL load or the

²The amount of SHO connections is controlled by adjusting the “addition window size” (*Reporting Range* in 3GPP specifications).

³Equation (13a) for $\beta = 1$.

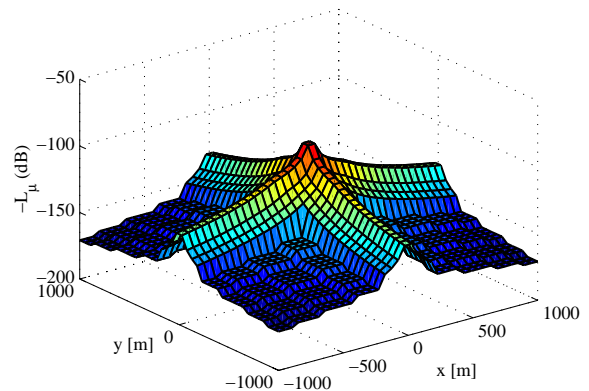


Figure 2: Microcell path losses for a cell site at (0,0), assuming an isotropic radiator as antenna.

maximum total DL transmit power have been exceeded.

3.2 Simulation Areas and Path Loss

Two different areas have been investigated, which are characterized by different sizes, cell positions and, most importantly, propagation models.

3.2.1 Area I: Hexagonal Cells and ETSI Path Loss

In Scenario I, hexagonal macrocell sites are arranged regularly in two tiers, with a single microcell being embedded in the central macrocell. The central macrocell thereby serves as a reference cell. Unless otherwise stated, three-sectorization has been studied. Macrocell path losses are computed according to the ETSI model ($L/dB = 128.1 + 37.6 \log_{10}(D)$) [6]. Microcell propagation losses are determined for a Manhattan-like environment similarly to the ETSI approach [6], Fig. 2 depicts the characteristics of this model.

3.2.2 Area II: Case Study

The second area represents downtown Dresden, Germany. The area of $2.3 \times 2.4 \text{ km}^2$ is characterized by a typically mixed urban building structure and comprises 13 Node Bs. The cell positions, sectorization and horizontal orientation of the 22 macrocells and 5 microcells correspond to those of existing GSM cells. Using a propagation prediction tool, the path losses from all antenna locations of the Node B sites to reference points in the area have been computed for $f = 2000 \text{ MHz}$.⁴

For the rest of the report, we will denote the two different simulation areas by Scenario I and Scenario II, respectively. The general results obtained for the widely accepted models in Scenario I will be compared to those obtained for the case study (Scenario II).

⁴Data provided by Mannesmann Mobilfunk GmbH.

4 OPTIMIZATION AND RESULTS

4.1 Macrocell Antenna and Downtilt

As a first important parameter, we investigated the effects of downtilting macrocell antennas. Microcells are omitted ($\nu_\mu = 0$), so that the achievable fractional macrocell load from equation (10) simplifies and obeys the well-known CDMA capacity relation

$$\nu_M \propto \frac{1}{1 + F_{MM}}. \quad (11)$$

The used sectorized antenna is a standard macrocell antenna for UMTS applications (65° , 18 dBi). The patterns for the various electrical tilt angles $\phi_M^{el} = \{0^\circ, \dots, 8^\circ\}$ have been obtained from measurements.⁵

Due to its high gain, the antenna exhibits a distinct vertical main lobe, which is oriented towards the horizon if no downtilt is applied. By downtilting the antenna, this lobe is directed below the horizon, and the received intercell interference originating from surrounding cells is correspondingly attenuated. This attenuation of intercell interference lowers the intercell-to-intracell interference ratio F_{MM} , which ultimately leads to an increase of the achievable fractional load of macrocells according to (11).

Fig. 3 shows the interference ratio F_{MM} for the central cell of Scenario I as a function of the antenna tilt angle, and Table 2 summarizes the related capacity gains.

The minimum interference ratios are obtained for the optimum tilt angle $\phi_M = 11^\circ$, at which neither the main lobe nor any side lobe of the vertical antenna pattern point towards the source of other-cell interference. Then the attenuation of the intercell-interference becomes maximum – a simple method of system-level interference suppression which eventually leads to an optimized capacity (Table 2).

This effect is likewise observable in Fig. 4, which displays the total number of users achieved in the simulations for downtown Dresden (Scenario II) for various downtilts and SHO addition window sizes. Again, the capacity is maximized for $\phi_M = 11^\circ$. Note that this equivalence of the optimum tilt angles for both areas occurs rather accidentally and is caused by the similar cell radii and antenna heights.

To state it explicitly: downtilting the antenna provides a strong potential for capacity optimization in systems with universal frequency reuse. The optimum occurs when the attenuation of intercell MAI is maximum, which is achieved by directing the

⁵Downtilts $\phi_M > 8^\circ$ are achieved by mechanically tilting the pattern valid for $\phi_M^{el} = 8^\circ$. Measurement data provided by Mannesmann Mobilfunk GmbH.

ϕ_M	Scenario I		Scenario II	
	Central cell	Total	Central cell	Total
3°	4%	5%	1%	1%
11°	61%	39%	24%	19%

Table 2: Capacity gains for pure macrocellular networks for various downtilts ϕ_M . The gains of the central cells and the total area are given with respect to a downtilt of $\phi_M = 0^\circ$; differences results from the limited number of cells and the corresponding incompleteness at the boundaries.

first significant null of the vertical antenna pattern towards the main source of other-cell interference. Unless otherwise stated, a downtilt of $\phi_M = 6^\circ$ was chosen for the following investigations.

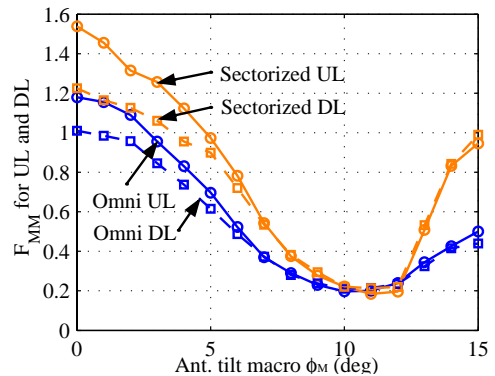


Figure 3: UL and DL intercell-to-intracell interference ratios F_{MM} for omni- and three-sectorization vs. the macrocell antenna downtilt in Scenario I. Downtilting antennas attenuates other-cell interference, so F decreases. The commonly assumed value $F_{MM} = 0.6$ is achieved for a downtilt of $\phi_M = 6^\circ \dots 7^\circ$.

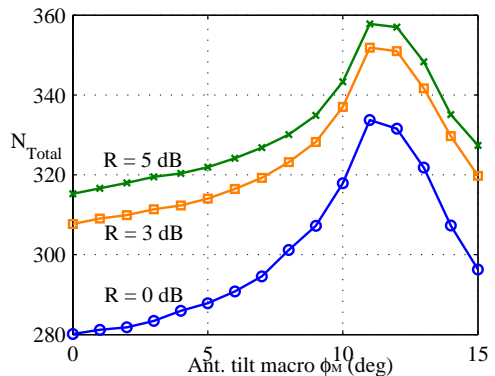


Figure 4: Achievable total number of users in the 22 macrocells of Scenario II vs. the antenna downtilt. Downtilting antennas attenuates intercell interference and hence increases capacity. SHO gains provide additional capacity improvements. Parameter: size of the soft handover addition window (R).

4.2 Uplink Load

A major issue discussed for the deployment of microcells in IS-95 is a *desensitization* [2] of the microcell receivers. Desensitization effectively demands higher transmit powers from microcell users, and thus reduces the susceptibility to interferences from

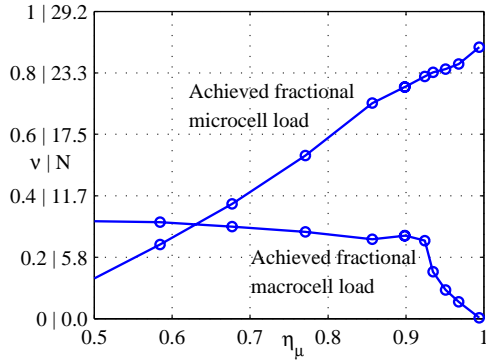


Figure 5: Achieved fractional load and number of users in the reference macrocell and microcell as a function of the allowed UL load in the microcell. Scenario I.

surrounding macrocells by making their contributions relatively less important. The similar concept of *power ratio control* [1] serves the same purpose: achieving a better interference isolation for smaller cells by adjusting higher intracell power levels.

While these concepts are the key enabler for capacity optimization in networks in which the power control mechanism is based on constant received power, the situation is different for networks with PC based on SINR, i.e. for UTRAN FDD systems. In the latter case, the users' transmit powers are automatically adapted to the actual interference situation. In connection with strong intercell MAI from macrocells (large $F_{\mu M}$), this may cause significantly higher interference levels in the microcells, and consequently leads to the question of the maximum allowed interference loading of microcells.

Admission control in the UTRAN FDD mode is based on the uplink load η , defined by

$$\eta = \frac{NR}{NR - 1} \quad (12)$$

where NR is the rise of the total received wideband interference power over the thermal noise floor, $NR = P_{I,tot}/P_{th}$. Please note carefully the differences between the two loading terms used here: ν_M and ν_μ represent the actual throughputs with respect to pole capacity that are achieved if the total received interference levels are limited according to η_M and η_μ .

The average UE transmit powers are related nonlinearly to the load η by $\overline{P}_{tx} \propto 1/(1 - \eta)$. That is, the transmission powers increase nonlinearly with the network's load. To guarantee coverage for transmit power limited mobiles, admission control ensures the load η_M to stay below a defined limit $\eta_{max,M}$ in macrocells. In microcells, however, mean path losses are lower than in the macrocellular environment, and capacity instead of coverage is the primary concern. An increased allowed interference load η_μ will therefore lead to a higher throughput ν_μ in the microcell. On the other hand, an extremely

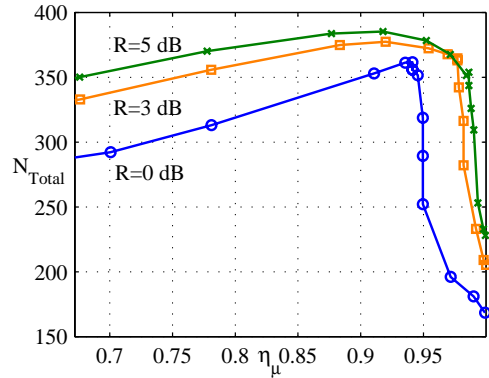


Figure 6: Achieved total number of users in the 22 macrocells and 5 microcells of Scenario II as a function of the max. allowed UL load in the microcell. Parameter: size of the soft handover addition window (R).

high UL load in the microcell may possibly deteriorate the interference situation in the surrounding cells ($F_{\mu M}$), and will consequently cause a degradation of both capacity and quality in the macro layer.

This tradeoff has been investigated by varying the maximum allowed UL load in the microcells, $\eta_{\mu,max}$. The key results are shown in Figures 5 and 6 for Scenario I and Scenario II, respectively. The first figure demonstrates how the capacity of the microcell increases as its load is allowed to rise, and how this increased microcell loading in turn affects the macrocell capacity. Note that the degradation of the macrocell capacity in Fig. 5 basically follows the characteristic of Fig. 1. In this example, a microcell capacity increase of 80% is attained by allowing the UL load to rise from 0.6 to 0.8. These improvements are achieved without significantly affecting macrocell performance.

Fig. 6 shows the influence of $\eta_{\mu,max}$ for multiple microcells on total system capacity in Scenario II. Parameter in this plot is the size of the soft handover addition window (R). A larger number of soft handover connections ($R > 0$ dB) not only improves total capacity due to the SHO gains, but also enables to control the throughput degradation for extremely high microcell loads more smoothly and hence allows to better exploit the potential of soft capacity.

In general, permitting a higher UL load in the microcell enables considerable capacity enhancements without necessarily having a substantial negative impact on macrocell efficacy. There is, however, the danger of a severe degradation of the overall capacity and quality if the microcell load is not well-controlled. This was the case for $\eta_{\mu,max} > 0.9$ in both areas.

4.3 Pilot Power Fraction

The cell size is directly related to the transmission power of the pilot channel as the cell search pro-

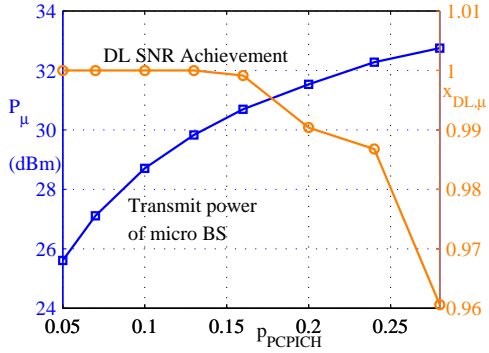


Figure 7: Total transmit power of the microcell (left axis) and DL SINR achievement (right axis) vs. the microcell pilot power fraction in Scenario I.

cedure selects the cell based on signal strength and SINR measurements of the Primary Common Pilot Channel (PCPICH).

In all simulations, 10% of the total available macrocell powers have been allocated to the pilots, and additionally 10% were assumed for the remaining common channels. In the microcells, a fraction p_{PCPICH} was allocated to the pilot; the total pilot and common channel power fraction was $2 \cdot p_{PCPICH}$.

The optimum cell shapes for non-regular positions of BSs are formed if all cells transmit their pilots with the same power. Varying the strength of the pilot shifts the cell border away from the site transmitting its pilot at a higher level. UEs near the former cell border will then be connected to a non-optimum cell in terms of path loss, thus increasing their transmit power and, consequently, intensifying interference.

The optimum situation with respect to mutual interferences is therefore achieved if the microcell pilot power corresponds to that of the surrounding macrocells, which is not feasible due to the low maximum output power of micro Node Bs. Hence, there is a tradeoff between more balanced interferences achieved by large microcell PCPICH powers and an adequate DL power budget accomplished by smaller PCPICH powers.

These effects are displayed in Figures 7 and 8. Fig. 7 shows how the total transmit power of the microcell approaches its maximum possible value of 33 dBm as the fraction p_{PCPICH} of the max. output power which is allocated to the pilot power is increased. The service area of the cell enlarges, and it becomes problematic to serve this area with the limited DL DCH power ($P_{max,\mu}^{DCH} = 20$ dBm). As a consequence, the fraction of DL connections that have reached their targets starts to drop (Fig. 7, right axis).

On the other hand, the large microcell service area caused by strong microcell pilots reduces the relative interferences from the surrounding macrocells, i.e. $F_{M\mu}$ decreases. Correspondingly, the mi-

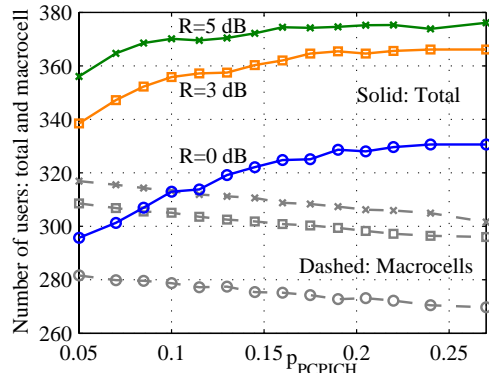


Figure 8: Achieved total number of users in Scenario II (22 macrocells, 5 microcells) and in the macrocells as a function of the microcell pilot power fraction p_{PCPICH} .

R [dB]	Total	Microcells	Macrocells
0	3.8%	45%	-1.3%
3	1.8%	21%	-1.4%
5	1.2%	15%	-1.4%

Table 3: Total capacity gains in Scenario II achieved by increasing the microcell pilot power fraction from 0.1 to 0.16 (column 2). Traffic redirection, i.e. the increased number of users in the microcells and the parallel reduction of the number of connections in the macrocell, are shown in columns 3 and 4, respectively. Parameter: size of the soft handover addition window (R).

crocell interference to the macrocell $F_{\mu M}$ increases. This balancing of the mutual interferences is reflected in an improvement of the total number of users that can be served. Fig. 8 shows this increase and the slight parallel reduction of the macrocell throughput.

The results in Table 3 imply that the overall capacity gains due to the variation of p_{PCPICH} are small, but that controlling the pilot power provides a strong means for redirecting traffic into microcells—an important feature of HCS systems.

4.4 Additional Parameters

4.4.1 Microcell Antenna and Downtilt

In addition to the small omnidirectional dipole antenna, which has been used for the microcell simulations so far, we investigated the performance of a small sectorized antenna (12 dBi). It was directed either towards or away from the closest macrocell. In contrast to the omnidirectional dipole, the sectorized antenna can be tilted and thus enables an attenuation of the interference contribution from and to the neighboring macrocells.

The corresponding microcell capacity gains for Scenario I and a microcell downtilt of 10° are at the order of 10% for various SHO addition window sizes. This holds for both antenna orientations.

4.4.2 Distance

Although the distance between a microcell and its surrounding macrocells may not be easily influenced, but is more or less given by radio network planning, it is of interest to investigate how the spatial separation affects the performance of the HCS system.

Surprisingly, the impact is lower than one might expect. If a microcell is located closely to a macrocell, the mutual interferences occur between these two cells, while otherwise multiple macrocells are involved. This was confirmed in a series of simulations.

It follows from this consideration, that there are no constraints for operating a microcell close to a macrocell, similar to the operation of multiple sectors per site on the same frequency. Hence, it is practicable to deploy the microcell exactly as required by the traffic hotspots.

4.5 Total Capacity Improvements

A comparison of four different scenarios in the Dresden region (Scenario II) is used to find the total capacity improvements achievable by deploying microcells with correspondingly adjusted parameters. Let scenario A describe a pure macrocellular system with a downtilt of $\phi_M = 3^\circ$. In scenario B, the macrocell downtilt is increased to $\phi_M = 11^\circ$. Microcells are then deployed in scenario C, whose parameters are set to the corresponding values of the macrocells (max. allowed load $\eta_{\mu,max} = 0.6$, $p_{PCPICH} = 0.1$). Finally, in scenario D these parameters are optimized according to the previously found results. Table 4 summarizes the settings and lists the resulting relevant figures of capacity.

Surprisingly, there is almost no capacity gain resulting from the deployment of the microcells if their parameters are not optimized (scenario C). The capacity of the system with microcells improves only if the parameters of the microcells are modified appropriately (scenario D). This vividly summarizes the importance of carefully choosing the parameters for a successful operation of the microcellular layer.

5 CONCLUSIONS

The influence of a number of important parameters on the joint deployment of macrocells and microcells has been studied for two different areas.

Firstly, it has been shown that reducing the intercell-to-intracell interference ratios by *downtilting antennas* provides significant capacity improvements for macrocellular networks.

Secondly, the strongest means for joint capacity optimization was provided by increasing the *allowed uplink load* in the microcell. That is, a higher allowed UL load in the microcell is crucial for taking full advantage of the microcell deployment. For

Scenario	A	B	C	D
Parameters				
Microcells	No	No	Yes	Yes
Macro tilt (ϕ_M)	3°	11°	11°	11°
Max. load $\eta_{\mu,max}$	N/A	N/A	0.6	0.85
Pilot (p_{PCPICH})	N/A	N/A	0.1	0.15
Results				
Macrocell users	319.5	357.8	362.2	350.3
Microcell users	0	0	4.6	50.9
Total users	319.5	357.8	366.8	401.2
Norm. Capacity	100%	112%	115%	126%

Table 4: Case study comparison. The results represent the attained number of users in the 22 macrocells and 5 microcells of the system. The normalized capacity in the last line is the total number of users achieved for the specific scenario divided by the total number of users attained in scenario A. $R = 5.0$ dB.

loads $\eta_{\mu} > 0.9$, however, instability in terms of diverging transmit powers governs the situation and leads to a loss of overall throughput and quality.

A large *pilot power* in microcells slightly increases their capacity. More importantly, the pilot power fraction provides a convenient means of interference balancing and traffic redirection. The gains that result from using *downtilted sectorized microcell antennas* instead of omnidirectional antennas have been discussed. Finally, the *distance* between a microcell and the closest macrocell has been found to have a low impact on overall performance.

ACKNOWLEDGEMENTS

The authors would like to thank P. Schneider, D2 Vodafone, for kindly providing the propagation data for the case study. Furthermore, we are grateful to K. Fligg for supplying the antenna measurement data.

REFERENCES

- [1] Dong Hee Kim, Dong Do Lee, Ho Joon Kim, and Keum Chan Whang, "Capacity analysis of macro/microcellular CDMA with power ratio control and tilted antenna," *IEEE Trans. Veh. Technol.*, vol. 49, pp. 34–42, Jan. 2000.
- [2] Joseph Shapira, "Microcell Engineering in CDMA Cellular Networks," *IEEE Trans. Veh. Technol.*, vol. 43, pp. 817–825, Nov. 1994.
- [3] Kari Sipilä, Mika Jäsberg, Jaana Laiho-Steffens, and Achim Wacker, "Soft Handover Gains in a Fast Power Controlled WCDMA Uplink," in *Proceedings of the 49th IEEE Veh. Technol. Conference*, 1999, vol. 2, pp. 1594–1598.
- [4] G.J. Foschini and Z. Miljanic, "A Simple Distributed Autonomous Power Control Algorithm and its Convergence," *IEEE Trans. Veh. Technol.*, vol. 42, pp. 641–646, Nov. 1993.
- [5] 3GPP, "3G TR 25.942 version 2.3.0, TSG RAN, RF System Scenarios (Release 1999)," Technical report, 3GPP, Sept. 2000.
- [6] ETSI, "3G TR 101 112 V3.2.0 (1998-04), Selection Procedures for the choice of radio transmission technologies for the UMTS (UMTS 30.03)," Technical report, ETSI, 1998.